01 Jun 2022

State-To-State Rate Coefficients for HCS^+ in Rotationally Inelastic Collisions with H2at Low Temperatures

Otoniel Denis-Alpizar

Ernesto Quintas-Sánchez
Missouri University of Science and Technology, quintassancheze@mst.edu

Richard Dawes
Missouri University of Science and Technology, dawesr@mst.edu

Recommended Citation

O. Denis-Alpizar et al., "State-To-State Rate Coefficients for HCS^+ in Rotationally Inelastic Collisions with H2at Low Temperatures," *Monthly Notices of the Royal Astronomical Society*, vol. 512, no. 4, pp. 5546 - 5551, Oxford University Press; Royal Astronomical Society, Jun 2022.
The definitive version is available at https://doi.org/10.1093/mnras/stac770

Monthly Notices of the ROYAL ASTRONOMICAL SOCIETY

MNRAS **512,** 5546–5551 (2022) https://doi.org/10.1093/mnras/stac770
Advance Access publication 2022 March 22

State-to-state rate coefficients for HCS^+ in rotationally inelastic collisions with H_2 at low temperatures

Otoniel Denis-Alpizar [1]★ Ernesto Quintas-Sánchez [2] and Richard Dawes [2]

[1]*Instituto de Ciencias Químicas Aplicadas, Facultad de Ingeniería, Universidad Autónoma de Chile, Av. Pedro de Valdivia 425, 7500912 Providencia, Santiago, Chile*
[2]*Department of Chemistry, Missouri University of Science and Technology, Rolla, MO 65409, United States*

Accepted 2022 March 16. Received 2022 March 6; in original form 2022 February 7

ABSTRACT

HCS^+ ions have been detected in several regions of the interstellar medium (ISM), but an accurate determination of the chemical-physical conditions in the molecular clouds where this molecule is observed requires detailed knowledge of the collisional rate coefficients with the most common colliders in those environments. In this work, we study the dynamics of rotationally inelastic collisions of $HCS^+ + H_2$ at low temperature, and report, for the first time, a set of rate coefficients for this system. We used a recently developed potential energy surface for the HCS^+–H_2 van der Waals complex and computed state-to-state rotational rate coefficients for the lower rotational states of HCS^+ in collision with both *para*- and *ortho*-H_2, analysing the influence of the computed rate coefficients on the determination of critical densities. Additionally, the computed rate coefficients are compared with those obtained by scaling the ones from HCS^+ in collision with He (an approximation that is sometimes used when data is lacking), and large differences are found. Furthermore, the approximation of using the rates for the $HCO^+ + H_2$ collision as a rough approximation for those of the $HCS^+ + H_2$ system is also evaluated. Finally, the complete set of de-excitation rate coefficients for the lowest 30 rotational states of HCS^+ by collision with H_2 is reported from 5 to 100 K.

Key words: astrochemistry – molecular data – molecular processes – scattering – ISM: molecules.

1 INTRODUCTION

The HCS^+ molecule has been widely observed in the interstellar medium (ISM) (Turner 1996; Rodríguez-Baras et al. 2021), being one of the species whose quantities are essential for obtaining elemental abundances in molecular clouds (Fuente et al. 2019). After its first detection in the Orion Nebulae (Thaddeus, Guélin & Linke 1981), HCS^+ molecules have been observed in a variety of ISM environments (Irvine, Good & Schloerb 1983; Turner 1996; Houde et al. 2000; Lucas & Liszt 2002; Nomura & Millar 2004; Leurini et al. 2006; Fuente et al. 2016; Potapov et al. 2016). This ion is formed in the ISM fundamentally by the reactions of CS^+ with H_2, C^+ with H_2S, and CS with H_3^+ and HCO^+ (McAllister 1978; Montaigne et al. 2005); while the main mechanism for its destruction is by reaction with electrons (Millar 1983). HCS^+ has shown to be non-reactive with most of the interstellar molecules at relevant collision energies, including H_2 (Millar et al. 1985).

In typical molecular clouds, temperatures range from five to a few tens of kelvins, and the densities range from 10^4 to $10^6\,cm^{-3}$ (Denis-Alpizar et al. 2020). Therefore, collisions are rare, and a Boltzmann distribution cannot describe the rotational population of the interstellar molecules in such environments. In such cases, analysis of the chemical-physical conditions of ISM regions where a molecule is observed should be performed using non-local thermal-equilibrium (non-LTE) models. But these models require knowledge of the Einstein coefficients, as well as the rotational rate coefficients of the observed molecules with the most common colliders in the ISM (i.e., H_2, He, H, and electrons). Moreover, since sulfur-containing molecules have not been observed in as much abundance as expected in the ISM (Rivière-Marichalar et al. 2019), accurate molecular data allowing a better estimation of the conditions where molecules such as HCS^+ are observed, are indeed valuable.

The collision of HCS^+ ions with He has been studied in detail by Monteiro (1984) and Dubernet, Quintas-Sánchez & Tuckey (2015). However, no set of rate coefficients has been reported so far for its collisions with H_2. When accurate molecular data is lacking, rate coefficients for the collision of a neutral molecule with H_2 are usually estimated by scaling from those obtained for collisions with He (Schöier et al. 2005). However, this is often not a good approximation, particularly in the case of ions, due to the different behaviour in the long range of the potential energy surface (PES). Also, in the LAMDA data base (Schöier et al. 2005; Van der Tak et al. 2020), the rates for $HCS^+ + H_2$ collisions are assumed to be the same as the ones obtained for HCO^+ (isovalent with HCS^+) by collisions with H_2; but the accuracy of this approximation deserves to be investigated.

Very recently, we reported (Quintas-Sánchez, Dawes & Denis-Alpizar 2021) the first PES for the HCS^+–H_2 van der Waals system. The global minimum of this surface is five times deeper than in the case of HCS^+–He, but is only half that found for HCO^+–H_2. Such large differences make it even more important to evaluate the approximations used so far for estimating the state-to-state rate coefficients for this system. The main goal of this work is to study the rotational relaxation of HCS^+ by H_2 at low temperatures and report

★ E-mail: otoniel.denis@uautonoma.cl

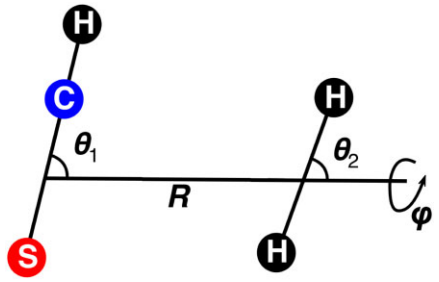

Figure 1. Internal coordinates used to describe the HCS$^+$ + H$_2$ system.

the first accurate set of rate coefficients for this collision system. The paper is organized as follows: in the next section, the methods employed are presented, while the results are discussed in Section 3. Finally, the conclusions are discussed and summarized in Section 4.

2 METHODS

In our previous work (Quintas-Sánchez et al. 2021), we presented the first theoretical spectroscopy and scattering study of the HCS$^+$–H$_2$ system. Using a new intermolecular PES, calculated for the ground electronic state of the complex, we computed the rovibrational bound states, rotational constants, as well as (de)-excitation cross-sections for the lowest levels in the collision of HCS$^+$ with both *para*- and *ortho*-H$_2$. Both the HCS$^+$ and H$_2$ molecules were considered as rigid rotors. In the case of linear triatomic molecules, close-coupling calculations including the bending motions have shown (Stoecklin et al. 2013; Denis-Alpizar, Stoecklin & Halvick 2014, 2015; Stoecklin, Denis-Alpizar & Halvick 2015) that the rigid rotor approximation is valid for collisional energies lower than the bending frequency. The HCS$^+$ molecule has a relatively large bending frequency of 784 cm^{-1} (Puzzarini 2005); therefore, close-coupling calculations for collisional energies lower – or slightly higher – than this value are expected to provide accurate results. The employed coordinates are shown in Fig. 1. R connects the centres of mass of the H$_2$ and HCS$^+$ molecules, while θ_1, θ_2, and φ describe the angular orientations of both systems.

Using the same highly accurate PES and state-of-the-art methods, in this paper we study the dynamics of HCS$^+$ rotational relaxation via collisions with both *para*- and *ortho*-H$_2$, focusing on the state-to-state rate coefficients at low temperatures. Details of the recently developed four-dimensional PES can be found in Quintas-Sánchez et al. (2021). Briefly, the analytical representation of the PES was constructed using an automated interpolating moving least-squares (IMLS) methodology, freely available as a software package under the name AUTOSURF (Quintas-Sánchez & Dawes 2019). The fitting basis and other aspects of the procedure were the same as for previous similar systems and have been described in detail elsewhere (Majumder, Ndengue & Dawes 2016; Dawes & Quintas-Sánchez 2018; Quintas-Sánchez & Dawes 2019, 2021). The surface was constructed from 3023 *ab initio* energies, computed with explicitly correlated coupled-cluster theory, CCSD(T)-F12b, (Knizia, Adler & Werner 2009) with two sizes of basis (VTZ-F12/VQZ-F12) (Peterson, Adler & Werner 2008) extrapolated to the complete basis set (CBS) limit. The final estimated root-mean-squared error was 0.19 cm^{-1}. The PES was found to have two minima defining the isomers of the system: a global minimum of −752.6 cm^{-1} in a T-shaped configuration, with the HCS$^+$ molecule acting as the stem of the T (with the H atom pointing to the H$_2$ molecule) and a centre-of-mass separation of 4.148 Å; and a secondary minimum of −509.1 cm^{-1} in a non-planar crossed structure, at a centre-of-mass separation of 3.341 Å. As mentioned in the previous section, the global minimum of this surface (−752.6 cm^{-1}) is five times deeper than in the case of HCS$^+$ + He [−138.5 cm^{-1}, Dubernet et al. (2015)], but is only half that found for HCO$^+$ + H$_2$ [−1509.4 cm^{-1}, Denis-Alpizar et al. (2020)]. Additionally – to facilitate comparison with the HCS$^+$ + He PES – the PESs of the HCS$^+$ + H$_2$ and HCO$^+$ + H$_2$ systems were averaged over the *para*-H$_2$ ($j = 0$) rotational wavefunction. Fig. 2 shows the two-dimensional (2D) plots of these averaged surfaces, as well as the surface of the HCS$^+$ + He complex. Here, not only the differences in the depth of the wells are observed, but also in the anisotropy of the PESs.

Because our quantum scattering calculations require an expansion of the angular dependence of the PES in products of spherical harmonics, the 4D IMLS potential was recast in that representation. First, the IMLS-PES was used to generate a grid of potential energies for 50 700 configurations. Then, the grid of energies were fitted following the same procedure recently used for studying the HCO$^+$–H$_2$ complex (Denis-Alpizar et al. 2020). Let us recall only the main features here . Briefly, the analytical function employed has the form:

$$V(R,\theta_1,\theta_2,\varphi) = \sum_{l_1=0}^{4}\sum_{l_2=0}^{10}\sum_{m=0}^{\min(l_1,l_2)} f_m^{l_1,l_2}(R) \times \bar{P}_{l_1}^m(\cos\theta_1)\bar{P}_{l_2}^m(\cos\theta_2)\cos(m\varphi) \quad (1)$$

where the angular part is represented by the multiplication of normalized associated Legendre polynomials and cosine functions. H$_2$ has a centre of symmetry; thus, l_1 is restricted to even values (Nasri et al. 2015). For each value of R, the energies were fitted using a least-squares method, with the weight function: $w(E) = \min(V_0/E;\ 10)$, where $V_0 = 5\,000$ cm^{-1}. Each coefficient $f_m^{l_1,l_2}(R)$ was then fitted using the Reproducing Kernel Hilbert Space (RKHS) procedure, so that (Ho & Rabitz 1996):

$$f_m^{l_1,l_2}(R) = \sum_{k=1}^{N} \alpha_k^{l_1,l_2,m} q^{2,2}(R, R_k)\,, \quad (2)$$

where N is the number of radial points of the grid $\{R_k\}$, and $q^{2,2}(R, R_k)$ are 1D kernels defined as:

$$q^{2,2}(R_k, R) = \frac{1}{3R_>^3} - \frac{R_<}{5R_>^4}, \quad (3)$$

where $R_>$ and $R_<$ are the greater and smaller values between R_k and R. The $\alpha_k^{l_1,l_2,m}$ coefficients are obtained by solving the system of linear equations $\mathbf{q}(\mathbf{R}_i, \mathbf{R}_j)\alpha = \mathbf{f}_m^{l_1,l_2}(\mathbf{R}_i)$, where i and j label the different radial geometrical configurations of the grid. The large number of energies in the grid, together with the use of the least-square and kernel procedure, allows a fit of high quality.

The dynamics of the collision of HCS$^+$ with *para*-H$_2$ and *ortho*-H$_2$ was studied using the Didimat code (Guillon et al. 2008). This code solves the close-coupling equations in the space-fixed frame. The log-derivative propagator (Manolopoulos 1988) was employed, and the maximum propagation distance was set to 100 a_0. The rotational constants of HCS$^+$ and H$_2$ were fixed to their experimental values: $B_{H_2} = 60.853$ cm^{-1} (Huber & Herzberg 1979) and $B_{HCS^+} = 0.71173$ cm^{-1} (Tang & Saito 1995).

The cross-sections from a given initial rotational state j of HCS$^+$ were computed for collisional energies in the $[10^{-2},\ 10^3]$ cm^{-1} interval. Up to $j = 20$, the basis included 35 rotational states of HCS$^+$, while for initial rotational states of HCS$^+$ from $j = 21$ up to $j = 30$, the basis was increased to include 40 states. Only one rotational state of H$_2$ was included in the basis for the close-coupling calculations.

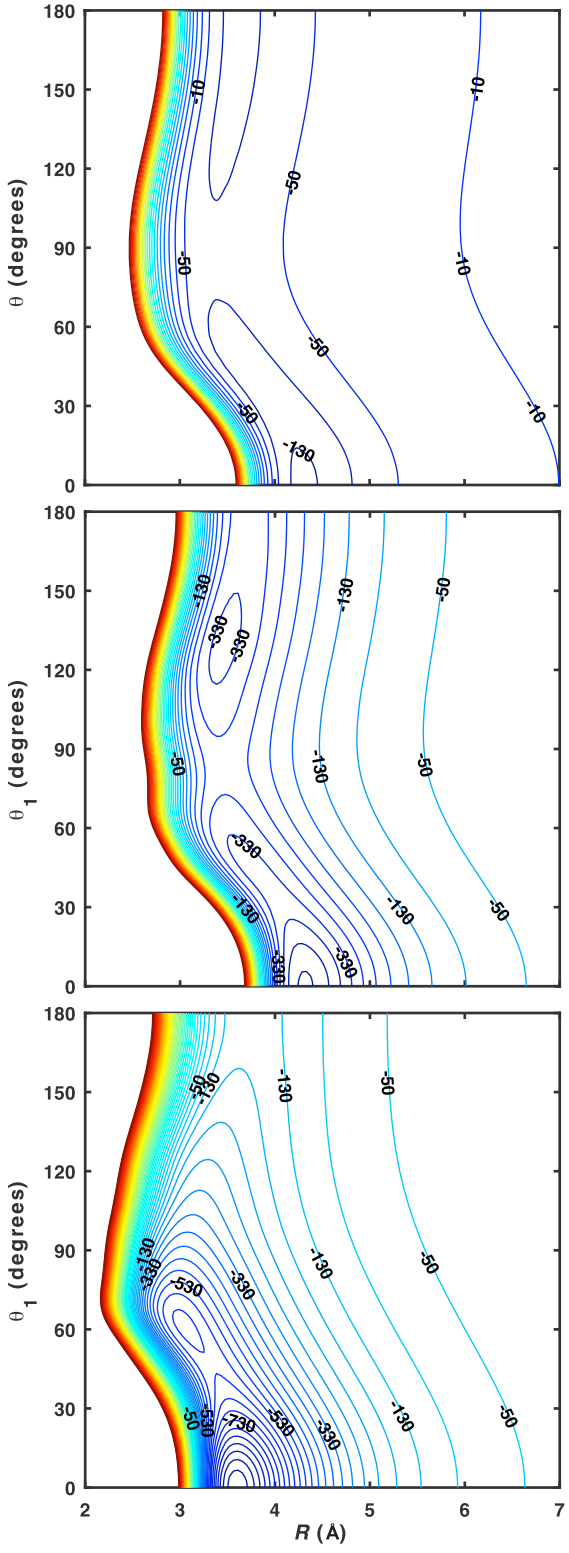

Figure 2. Comparison of the PESs for the HCS^+–He (upper panel), HCS^+–H_2 (middle panel), and HCO^+–H_2 (lower panel) systems. The angle describes the orientation of the HCS^+ or HCO^+ fragment. Contours are separated by 40 cm^{-1}. The HCS^+–H_2 and HCO^+–H_2 PESs were averaged over the *para*-H_2 wavefunction, see text for details.

The small influence – in the scattering calculation – of the number of rotational states of H_2 included in the basis was discussed in our previous paper (Quintas-Sánchez et al. 2021). The convergence of the quenching cross-sections is checked automatically by the code as a function of the total angular momentum (J) for each collision energy. At the highest collisional energy, 1000 cm^{-1}, the maximum value of J needed to reach convergence was $J = 99$.

Finally, the state-to-state de-excitation rate coefficients ($k_{j_i \to j_f}$) are computed by the average of the rotational cross-sections ($\sigma_{j_i \to j_f}$) over a Maxwell–Boltzmann distribution at a given temperature T, as

$$k_{j_i \to j_f}(T) = \sqrt{\frac{8}{\pi \mu k_B^3 T^3}} \int_0^\infty E_c \, \sigma_{j_i \to j_f}(E_c) \, e^{-\frac{E_c}{k_B T}} \, dE_c \,, \tag{4}$$

where j_i and j_f are the initial and final rotational states of HCS^+, E_c is the collisional energy, and k_B is the Boltzmann constant.

3 RESULTS AND DISCUSSION

Rotational de-excitation cross-sections of HCS^+ in collision with *para*- (solid lines) and *ortho*-H_2 (dashed lines) are shown in Fig. 3 from the initial rotational states $j = 7$ (upper panel), $j = 6$ (middle panel), and $j = 5$ (lower panel). Note that in the figure a logarithmic scale is used for both the x- and y-axes. The curves show typical shape- and Feshbach-resonances for van der Waals systems, which are associated with the formation of quasi-bound states due to the effective potential and the coupling between open and closed channels. As expected, all cross-sections decrease with increasing collision energy and decrease for larger increments of Δj. It should be noted that the calculations were carried out up to 1000 cm^{-1} because, at collisional energies higher than the opening of the first excited vibrational level of the triatomic molecule, the bending–rotation coupling could affect the magnitude of the cross-sections, as was observed for the C_3 +H_2 collision system (Stoecklin et al. 2015). Future work in this direction would be valuable.

As can be seen in Fig. 3, the similarities in the de-excitation cross-sections by collision with *para*-H_2 and *ortho*-H_2 observed for $j < 4$ in our preliminary study (Quintas-Sánchez et al. 2021) remain for larger values of j. Comparing the *para*-H_2 and *ortho*-H_2 cross-sections, the results converge to be quite similar at higher collision energies (especially above 100 cm^{-1}), while pronounced differences are observed at lower energies. It is also worth noticing that for most transitions, the cross-sections for collision with *ortho*-H_2 are appreciably larger – noticeable even on the log-scale plot – for energies below 50 cm^{-1}. At 10 K, the ratio between the rates for *para*- and *ortho*-H_2, including all de-excitation transitions from the initial rotational states $j = 1$ to $j = 7$, varies from 1.1 to 1.6 (with an average value of 1.2), while at 100 K, this value ranges from 1.0 to 1.2 (with an average value of 1.09). Such general behaviour has been also found in several studies of other ions in collisions with H_2; *e.g.*, HCO^+ (Denis-Alpizar et al. 2020), DCO^+ (Denis-Alpizar et al. 2020), N_2H^+ (Balança et al. 2020), SH^+ (Dagdigian 2019), CF^+ (Desrousseaux et al. 2019), C_3N^- (Lara-Moreno, Stoecklin & Halvick 2019), C_6H^- (Walker et al. 2017), and CN^- (Kłos & Lique 2011). This was discussed in detail by Lara-Moreno et al. (2019) for the C_3N^- + H_2 system, and the similarities were attributed to the features of the short-range interaction. This interaction appears to be dominated by the attractive isotropic term of the PES, A_{00}^0, which gives non-zero contributions in the coupling matrix element [see *e.g.* Eq. 9 from Green (1975)] for both *para*-H_2 ($j = 0$) and *ortho*-H_2 ($j = 1$). Henceforth, we will focus only on the rate coefficients of HCS^+ in collisions with *para*-H_2.

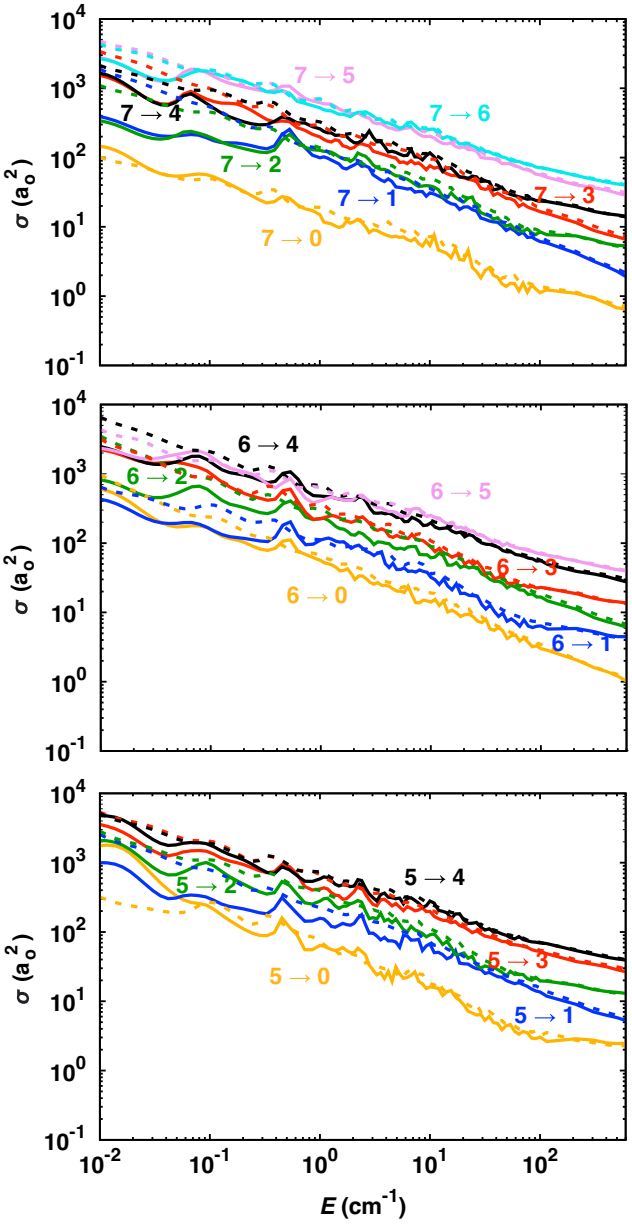

Figure 3. Rotational de-excitation cross-sections of HCS$^+$ in collision with *para*- (solid lines) and *ortho*-H$_2$ (dashed lines) from $j_i = 7$ (upper panel), $j_i = 6$ (middle panel), and $j_i = 5$ (lower panel). Rotational transitions of HCS$^+$ are labelled as $j_i \rightarrow j_f$.

Here, we address two assumptions often used as approximations to estimate rate coefficients for collisions with H$_2$ when no other – more accurate – theoretical data is available, namely: (i) the use of a mass scaling factor applied to data obtained for collisions with He; and (ii) to substitute the species of interest (in this case, HCS$^+$) by a 'similar' molecule for which such data is previously known (in this particular case, its isovalent ion HCO$^+$).

Table 1 shows the rate coefficients computed in this work – at several temperatures, for different $j \rightarrow j'$ transitions – and those reported for the collision with He (Dubernet et al. 2015). The use of a mass scaling factor for estimating the rate coefficients for the collision with *para*-H$_2$ from those with He is a very common approximation in the absence of rates with H$_2$. However, as shown in the table, for this system, the ratio of accurate data $k_{j\rightarrow j'}^{\mathrm{HCS^+}+\mathrm{H_2}}/k_{j\rightarrow j'}^{\mathrm{HCS^+}+\mathrm{He}}$ varies from 1.9 to 6.9, while only a factor of 1.4 would be applied using this approximation (Schöier et al. 2005). The maximum differences are observed at very low temperatures; but even at 60 K, the average ratio is 2.6. Therefore, using the mass scaling factor is not a good approximation – even on average – for HCS$^+$ + H$_2$ collisions. This is not too surprising as the long-range behaviour of the PES for the collision of an ion with He is dominated by the induction term (which has only an R^{-4} dependence), while for the case of collisions with H$_2$, the long-range interaction is dominated by the electrostatic charge–quadrupole term (which has an R^{-3} dependence). A full set of rate coefficients for the collision of HCS$^+$ with H$_2$ can be found in the supplementary materials.

The LAMDA data base (Schöier et al. 2005), given the lack of data for HCS$^+$, takes the rates for HCS$^+$ + H$_2$ to be the same as for HCO$^+$ + H$_2$ collisions. However, this is not an accurate approximation, as Fig. 4 clearly illustrates. Furthermore, Fig. 4 shows that the rates decrease with increasing $|\Delta j|$ and a typical $|\Delta j| = 1$ propensity for collision with non-homonuclear molecules such as HCS$^+$ is also observed. This propensity was also observed in collisions with He, *cf.* Table 1.

The astrophysical implications of the new set of rate coefficients obtained here can be explored by determining the critical densities ($\eta_c^{(j)}$), i.e. the density of H$_2$ for which radiative and collisional de-excitation processes are equally important. For densities much larger than these critical values, the LTE model can be accurately applied. At a given temperature, the critical density can be determined as (Yazidi, Ben Abdallah & Lique 2014):

$$\eta_c^{(j)}(T) = \frac{A_{j\rightarrow j-1}}{\sum\limits_{j'<j} k_{j\rightarrow j'}(T)}\,, \tag{5}$$

where $k_{j\rightarrow j'}$ is the rotational rate coefficient for the $j \rightarrow j'$ transition, and $A_{j\rightarrow j-1}$ is the Einstein coefficient for the de-excitation between the states j and $j-1$.

Table 2 shows $\eta_c^{(j)}$ at 10 and 60 K for $\Delta j = -1$ transitions from the lower rotational states of HCS$^+$. The critical density has a weak dependence on T (at least for low temperatures), as was previously noticed for the rates, *cf.* Fig. 4. The values of $\eta_c^{(j)}$ obtained using the rates for HCO$^+$ + H$_2$, and those scaled from HCS$^+$ + He collisions, are also included in Table 2. Both approximations are shown to be inaccurate. If the rates for HCO$^+$ + H$_2$ are used, $\eta_c^{(j)}$ is underestimated by up to a factor of 2.3. If the rates employed are those scaled from HCS$^+$ + He, $\eta_c^{(j)}$ is overestimated up to a factor of 2.2. This is because the scaled rates are too small and appear in the denominator of equation (5). Therefore, it is clearly preferable to employ accurate system-specific rates for non-LTE modelling of this system instead of those scaled from HCS$^+$ + He collisions or calculated for the HCO$^+$ + H$_2$ system.

4 SUMMARY AND CONCLUSIONS

Using a recently developed PES for the HCS$^+$–H$_2$ van der Waals system, a quantum scattering study of the rotational relaxation of HCS$^+$ ions by collisions with H$_2$ was performed at the rigorous close-coupling level. This work expands on our previous study of this system, reporting extensive results at low temperature. Similarities between the rotational de-excitation rate coefficients of HCS$^+$ by *para*- and *ortho*-H$_2$ were found for higher collision energies (especially above 100 cm^{-1}), while pronounced differences were observed at very low energies. The astrophysical implications of the computed set of rate coefficients were explored by determining the critical densities. Furthermore, two common approximations to

Table 1. Rotational de-excitation rate coefficients (in $cm^3 molecule^{-1} s^{-1}$) of HCS^+ in collision with H_2 at several temperatures for different $j \rightarrow j'$ transitions. The rate coefficients for $HCS^+ + He$ collisions reported by (Dubernet et al. 2015), and the corresponding ratio ($k^{HCS^+-H_2} / k^{HCS^+-He}$, comparable to the approximate factor of 1.4) are also included. A full set of rotational rate coefficients of HCS^+ by collisions with H_2 can be found in the supplementary materials.

		$T = 10$ K			$T = 20$ K			$T = 60$ K		
j	j'	$k^{HCS^+-H_2}$	k^{HCS^+-He}	Ratio	$k^{HCS^+-H_2}$	k^{HCS^+-He}	Ratio	$k^{HCS^+-H_2}$	k^{HCS^+-He}	Ratio
1	0	1.07×10^{-10}	4.89×10^{-11}	2.2	1.02×10^{-10}	5.12×10^{-11}	2.0	1.10×10^{-10}	5.71×10^{-11}	1.9
2	0	5.43×10^{-11}	2.22×10^{-11}	2.4	5.38×10^{-11}	2.45×10^{-11}	2.2	5.95×10^{-11}	2.94×10^{-11}	2.0
2	1	2.18×10^{-10}	8.15×10^{-11}	2.7	1.93×10^{-10}	8.15×10^{-11}	2.4	1.82×10^{-10}	8.70×10^{-11}	2.1
3	0	3.27×10^{-11}	8.19×10^{-12}	4.0	2.83×10^{-11}	9.00×10^{-12}	3.1	2.53×10^{-11}	1.05×10^{-11}	2.4
3	1	1.14×10^{-10}	3.99×10^{-11}	2.9	1.10×10^{-10}	4.28×10^{-11}	2.6	1.14×10^{-10}	4.89×10^{-11}	2.3
3	2	2.14×10^{-10}	7.96×10^{-11}	2.7	2.05×10^{-10}	8.27×10^{-11}	2.5	2.02×10^{-10}	9.08×10^{-11}	2.2
4	0	2.34×10^{-11}	3.38×10^{-12}	6.9	2.18×10^{-11}	3.85×10^{-12}	5.7	2.01×10^{-11}	4.92×10^{-12}	4.1
4	1	7.64×10^{-11}	1.59×10^{-11}	4.8	6.52×10^{-11}	1.75×10^{-11}	3.7	5.53×10^{-11}	1.97×10^{-11}	2.8
4	2	1.54×10^{-10}	5.46×10^{-11}	2.8	1.47×10^{-10}	5.69×10^{-11}	2.6	1.47×10^{-10}	6.01×10^{-11}	2.4
4	3	2.13×10^{-10}	8.04×10^{-11}	2.6	2.06×10^{-10}	8.45×10^{-11}	2.4	2.06×10^{-10}	9.22×10^{-11}	2.2
5	0	1.64×10^{-11}	2.78×10^{-12}	5.9	1.39×10^{-11}	2.96×10^{-12}	4.7	1.10×10^{-11}	3.33×10^{-12}	3.3
5	1	5.45×10^{-11}	8.12×10^{-12}	6.7	5.20×10^{-11}	9.31×10^{-12}	5.6	4.64×10^{-11}	1.06×10^{-11}	4.4
5	2	8.44×10^{-11}	1.89×10^{-11}	4.5	7.39×10^{-11}	2.10×10^{-11}	3.5	6.52×10^{-11}	2.28×10^{-11}	2.9
5	3	1.68×10^{-10}	6.43×10^{-11}	2.6	1.66×10^{-10}	6.63×10^{-11}	2.5	1.62×10^{-10}	6.81×10^{-11}	2.4
5	4	2.17×10^{-10}	8.59×10^{-11}	2.5	2.14×10^{-10}	9.03×10^{-11}	2.4	2.12×10^{-10}	9.51×10^{-11}	2.2

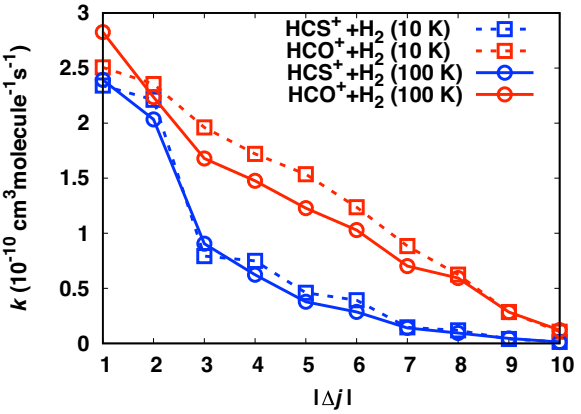

Figure 4. Rotational rate coefficients of HCS^+ in collision with H_2 at 10 and 100 K from $j = 10$. The rates for $HCO^+ + H_2$ are also included.

Table 2. Critical densities (in $10^4\,cm^{-3}$) for $\Delta j = -1$ transitions of the HCS^+ molecule obtained using the rate coefficients computed in this work, at 10 and 60 K, are compared with those scaled from $HCS^+ + He$ collisions, and with those obtained for the $HCO^+ + H_2$ system.

j_i	j_f	HCS^++H_2	HCS^++He (scaled)	HCO^++H_2
		$T = 10$ K		
1	0	1.08	1.69	0.47
2	1	4.08	7.64	1.98
3	2	11.12	22.45	4.79
4	3	21.15	45.66	9.70
5	4	36.47	78.17	17.88
6	5	58.85	83.25	28.99
		$T = 60$ K		
1	0	1.05	1.45	0.59
2	1	4.60	6.81	2.54
3	2	11.76	19.08	6.41
4	3	23.05	39.82	12.20
5	4	39.66	70.38	21.32
6	5	62.44	113.86	34.05

estimate the rate coefficients when specific data is lacking were evaluated: scaling the ones obtained from HCS^+ in collision with He, and the use of the rates for $HCO^+ + H_2$ as a proxy for $HCS^+ + H_2$. Both approximations proved to be inaccurate for this case. Finally, a complete set of rate coefficients for the lowest 30 rotational states of HCS^+ in collisions with H_2 is reported between 5 and 100 K. These data will help inform models and data bases relevant to ISM chemistry.

ACKNOWLEDGEMENTS

Support from the project CONICYT/FONDECYT/REGULAR /N°1200732 is gratefully acknowledged. RD and EQ-S are supported by the U.S. Department of Energy (Award DE-SC0019740). Computing resources were supported by the National Science Foundation under Grant No. OAC-1919789.

DATA AVAILABILITY

The data underlying this article are available in the article and in its online supplementary material.

REFERENCES

Balança C., Scribano Y., Loreau J., Lique F., Feautrier N., 2020, MNRAS., 495, 2524
Dagdigian P. J., 2019, MNRAS, 487, 3427
Dawes R., Quintas-Sánchez E., 2018, in Parrill A. L., Lipkowitz K. B., eds, The Construction of Ab Initio-Based Potential Energy Surfaces, Reviews in Computational Chemistry. John Wiley & Sons, Ltd, New Jersey, USA
Denis-Alpizar O., Stoecklin T., Halvick P., 2014, J. Chem. Phys., 140, 084316
Denis-Alpizar O., Stoecklin T., Halvick P., 2015, MNRAS, 453, 1317
Denis-Alpizar O., Stoecklin T., Dutrey A., Guilloteau S., 2020, MNRAS, 497, 4276
Desrousseaux B., Quintas-Sánchez E., Dawes R., Lique F., 2019, J. Phys. Chem. A, 123, 9637
Dubernet M.-L., Quintas-Sánchez E., Tuckey P., 2015, J. Chem. Phys., 143, 044315
Fuente A. et al., 2016, A&A, 593, A94
Fuente A. et al., 2019, A&A., 624, A105

Green S., 1975, J. Chem. Phys., 62, 2271
Guillon G., Stoecklin T., Voronin A., Halvick P., 2008, J. Chem. Phys., 129, 104308
Ho T.-S., Rabitz H., 1996, J. Chem. Phys., 104, 2584
Houde M., Peng R., Phillips T. G., Bastien P., Yoshida H., 2000, ApJ, 537, 245
Huber K. P., Herzberg G., 1979, Molecular Spectra and Molecular Structure. IV. Van Nostrand Reinhold, New York
Irvine W. M., Good J., Schloerb F., 1983, A&A, 127, L10
Kłos J., Lique F., 2011, MNRAS, 418, 271
Knizia G., Adler T. B., Werner H.-J., 2009, J. Chem. Phys., 130, 054104
Lara-Moreno M., Stoecklin T., Halvick P., 2019, MNRAS, 486, 414
Leurini S. et al., 2006, A&A, 454, L47
Lucas R., Liszt H., 2002, A&A, 384, 1054
McAllister T., 1978, ApJ, 225, 857
Majumder M., Ndengue S. A., Dawes R., 2016, Mol. Phys., 114, 1
Manolopoulos D. E., 1988, PhD thesis, Univ. Cambridge
Millar T., 1983, MNRAS, 202, 683
Millar T., Adams N., Smith D., Clary D., 1985, MNRAS, 216, 1025
Montaigne H. et al., 2005, ApJ, 631, 653
Monteiro T., 1984, MNRAS, 210, 1
Nasri S., Ajili Y., Jaidane N.-E., Kalugina Y. N., Halvick P., Stoecklin T., Hochlaf M., 2015, J. Chem. Phys., 142, 174301
Nomura H., Millar T., 2004, A&A, 414, 409
Peterson K. A., Adler T. B., Werner H.-J., 2008, J. Chem. Phys., 128, 084102
Potapov A., Sánchez-Monge Á., Schilke P., Graf U., Möller T., Schlemmer S., 2016, A&A, 594, A117
Puzzarini C., 2005, J. Chem. Phys., 123, 024313
Quintas-Sánchez E., Dawes R., 2019, J. Chem. Inf. Model., 59, 262
Quintas-Sánchez E., Dawes R., 2021, Annu. Rev. Phys. Chem., 72, 399
Quintas-Sánchez E., Dawes R., Denis-Alpizar O., 2021, Mol. Phys., 119, e1980234
Rivière-Marichalar P. et al., 2019, A&A, 628, A16
Rodríguez-Baras M. et al., 2021, A&A, 648, A120
Schöier F. L., van der Tak F. F. S., van Dishoeck E. F., Black J. H., 2005, A&A, 432, 369
Stoecklin T., Denis-Alpizar O., Halvick P., Dubernet M.-L., 2013, J. Chem. Phys., 139, 124317
Stoecklin T., Denis-Alpizar O., Halvick P., 2015, MNRAS, 449, 3420
Tang J., Saito S., 1995, ApJ, 451, L93
Thaddeus P., Guélin M., Linke R., 1981, ApJ, 246, L41
Turner B., 1996, ApJ, 461, 246
Van der Tak F. F., Lique F., Faure A., Black J. H., van Dishoeck E. F., 2020, Atoms, 8, 15
Walker K. M., Lique F., Dumouchel F., Dawes R., 2017, MNRAS, 466, 831
Yazidi O., Ben Abdallah D., Lique F., 2014, MNRAS, 441, 664

SUPPORTING INFORMATION

Supplementary data are available at *MNRAS* online.

Please note: Oxford University Press is not responsible for the content or functionality of any supporting materials supplied by the authors. Any queries (other than missing material) should be directed to the corresponding author for the article.

This paper has been typeset from a TEX/LATEX file prepared by the author.